Optimal scanning strategy for on-machine inspection with laser-plane sensor

Nguyen Duy Minh Phan, Yann Quinsat, Claire Lartigue

Noname manuscript No.
(will be inserted by the editor)

Optimal scanning strategy for on-machine inspection with laser-plane sensor

Nguyen Duy Minh Phan · Yann Quinsat · Claire Lartigue

Received: date / Accepted: date

Abstract The purpose of this paper is to propose a scan path planning method for on-machine measurement (OMM) in a 5-axis machine-tool. Sensor accessibility can be enhanced using the 5 degrees of freedom and the spindle rotation. The laser-plane sensor replacing the cutting tool in the spindle enables to reduce the measurement time and thus allows for rapid decision-making concerning the geometrical conformity of manufactured parts and potential machining corrections. The scan path planning is based on the control of the overlap between two consecutive passes by managing the orientations and the coverage rate of laser beam. Therefore, both scanning quality and scanning time can be controlled by optimizing the overlap zones. In this paper, we adapt the method previously developed for 6-axis robots to a 5-axis machine-tool.

Keywords On-Machine Measurement (OMM) · Laser-plane sensor · Scan path planning · Overlap · 5-axis machine-tool

1 Introduction

On-Machine Measurement (OMM) is a set of measurement techniques performed while the part is still located in the machine-tool. Because the machine-tool holds the sensor and allows sensor displacements like on classical Coordinate Measuring

M. Phan
LURPA, ENS Paris-Saclay, Univ. Paris-Sud, Université Paris-Saclay, 94235 Cachan, France ;
The University of Danang- University of Technology and Education, 550 000 Danang, Vietnam
E-mail: nguyen-duy-minh.phan@ens-paris-saclay.fr - pndminh@ute.udn.vn

Y. Quinsat
LURPA, ENS Paris-Saclay, Univ. Paris-Sud, Université Paris-Saclay, 94235 Cachan, France
Tel.: +33147402213
Fax: +33147402220
E-mail: yann.quinsat@ens-paris-saclay.fr

C. Lartique
LURPA, ENS Paris-Saclay, Univ. Paris-Sud, Université Paris-Saclay, 94235 Cachan, France
E-mail: claire.lartigue@ens-paris-saclay.fr

Machines [8], the machining process is stopped. OMM allows for rapid decision-making about part geometry confomity, and potential machining process corrections. These techniques are completely included in the manufacturing metrology roadmap for "Industrie 4.0" defined by Imkap et al. [5]. Although touch probes still remain the standard for OMM, the use of laser-plane sensor has become more and more popular for part geometry measurements due to its ability to deliver a great number of points in a short time with relatively good uncertainty [28]. However, few works have dealt with the generation of on-machine scanning paths using laser-plane sensors well-adapted for machine-tools. The first reason for this gap is that it is difficult to integrate a laser sensor into a machine-tool, and another difficulty is to generate scanning strategies that include quality control. The work proposed in this paper deals with a methodology for the generation of on-machine scanning paths using a laser-plane sensor efficient for measurement on a 5-axis machine-tool.

1.1 Related works

During on-machine measurement (OMM), the measurement of part geometry is performed without removing the part from its set-up when the machining process is stopped. This facilitates the comparison of the machined part geometry to its CAD model. Contact systems such as tactile probes are most commonly used, and make it possible to use the machine tool instead of a coordinate measuring machine [8]. In [9], measurement uncertainties of the machine-tool are well identified, and the use of OMM allows to check the position of the part in the set-up or to identify the part geometry after machining. Cho et al. [1] propose an *on-machine* probing strategy for parts with complex shapes. The tool trajectory which machines the surface is used in order to generate the touch probe trajectory. It is thus possible not to measure the cusp heights, and to avoid disturbing the measurement. More recently Huang et. al. [3] proposed to control the machining process during the production of thin-walls, using on-machine measurements. In the context of multi-axis machining, Zhao et al. [21] demonstrated the benefit of managing the machine configurations in order to better control the measurement quality.

While non-contact systems allow a good compromise between acquisition speed and measurement quality for the measurement of complex shape parts [17, 19], there has been little work on their use for on-machine measurements in the context of multi-axis machine-tools. Nishikawa et al. [10] indicate that the use of a laser sensor in a multi-axis machine yields quite similar results to the measurements of turbine blade sections obtained on a CMM. Ibaraki et al. [4] also use a laser displacement sensor to measure different profiles on an axi-symmetrical part. To improve quality, they propose a kinematic model of the machine which brings out each contribution of various types of errors affecting the measurement with the aim of improving quality. These different works focus on the sensor displacement only to measure the altitude of a point in the sensor frame. To increase the amount of acquired data and to reduce measurement time, laser-plane sensors are interesting as their dimensional characteristics simplify their integration on machine-tools. Neverteless, there are few examples in the literature of their use, and they are generally limited to 3-axis trajectories. For instance, Poulhaon et al. [13] use such a sensor to generate adaptive machining trajectories in a 3-axis machining context.If

this work is interesting for in-situ measurements, there has not been yet any specific work on an generation of measurement trajectories with a laser sensor adapted to the on-machine context.

1.2 Scan path planning with laser-plane sensor

The scan path (or scanning trajectory) is a set of sensor configurations (positions and orientations) $(C_E; \mathbf{V_L}; \mathbf{V_C})$, for which the driven point C_E positions the laser line in the field of view (FOV), and the couple of vectors $\mathbf{V_L}; \mathbf{V_C}$) orients the scanner line, with $\mathbf{V_C}$ the director vector of the light-beam axis, and $\mathbf{V_L}$, the director vector of the scanning line (Figure 1).

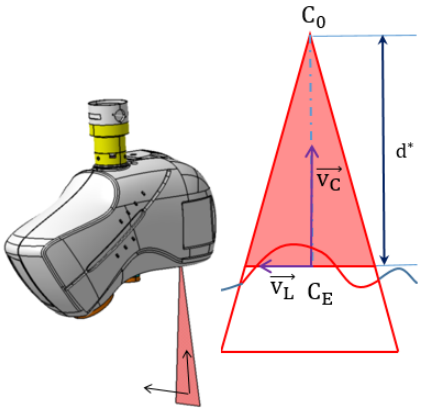

Fig. 1 Sensor Parameterisation

The scanning strategy, which consists in defining the scan path as a succession of view points, generally relies on various constraints. In the literature, visibility constraints were first introduced [23,24,20]. Indeed, to be scanned, the surface must be visible by the sensor without occultation, that means belonging to the field of view defined by the different components of the sensor (laser source, camera(s)).

Visibility contraints were then completed by quality constraints, such as measuring noise and/or accuracy. Data quality is mainly related to the scanning distance, along with the sensor's orientation relatively to the digitized surface [18, 15] but also depends on factors such as the overlap between sucessive paths [12, 15]. If some works can be found in the literature concerning trajectory planning with quality considerations for CMMs [27] or for displacement systems offering more degrees of freedom (such as robots) [2,22,26], little works have addressed scan path planning for in-situ measurement with 5-axis machine tools (OMM). OMM implies some other constraints linked to measuring time. As the machining process is stopped during the measurement stage, this involves a loss of machine availability during this stage. As a result, scan path planning turns out to be es-

sential to the success of OMM. A critical element concerns the compromise that must be found between measuring time and quality.

Within this context, this paper deals with an original trajectory planning method for laser-plane sensor measurements well-adapted to 5-axis machine tools. The originality lies in the fact that the trajectory allows not only to take scanning quality constraints into account, but also to minimize the time allocated to the measurement operation. The proposed method has been enterely developped and assessed on an industrial CNC machine tool.

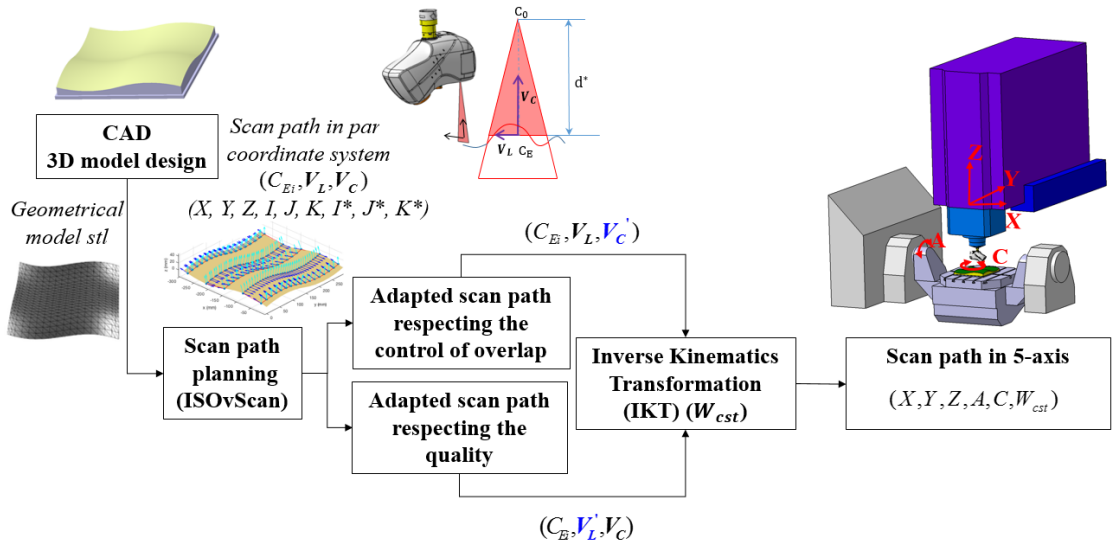

Fig. 2 Proposed method

In a previous work, we developed a method that integrates the control of overlap as an additional quality criterion, and that proved to be efficient for scanner path planning on industrial robots [12]. The method, ISOvScan, generates a scanning trajectory which is well-adapted to a structure with 6 dof (degrees of freedom) and which can be adjusted to a 5-axis machine-tool. Indeed, the trajectory expressed in the part frame as a set of coordinates $(X, Y, Z, I, J, K, I^*, J^*, K^*)$ is expressed in the machine-tool frame thanks to the Inverse Kinematics Transformation (IKT). In the case of a RRTTT machine tool, the IKT leads to the set of coordinates (X, Y, Z, A, C, W) in the articular space where A and C are the classical angles, and where W enables spindle indexation. The main difficulty here is that the spindle indexation cannot be continuously controlled between two scanner configurations. It is thus necessary to fix the spindle indexation to a constant value W_{cst} for all the scanner configurations (Figure 2). The initial trajectory must thus be modified consequently.

This paper is organized as follows. The scan path planning method, ISOvScan, is briefly presented in Section 2. Section 3 presents our approach to adapt the trajectory to 5-axis scanning on a machine-tool. Section 4 is dedicated to the application of the proposed method to a test case, and its implementation on an industrial CNC machine-tool. Some conclusions are drawn in the last section.

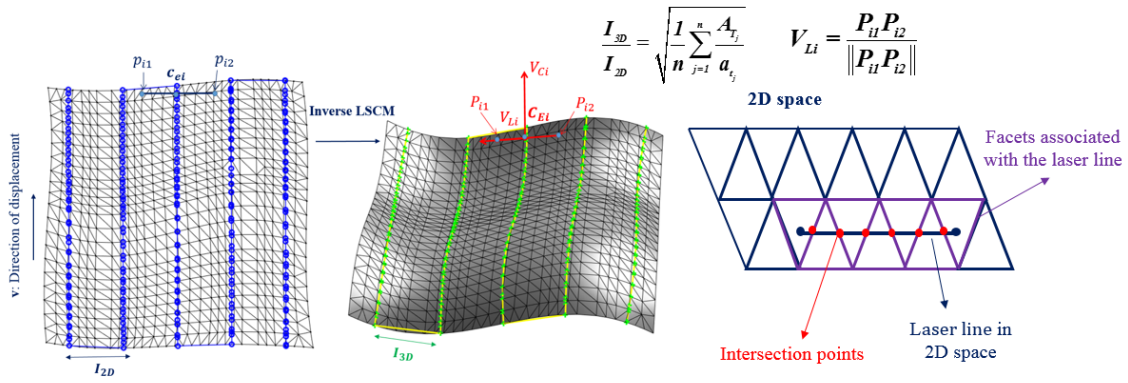

Fig. 3 Calculation of the scan trajectory

2 ISOvScan: Scan path planning method

In a previous work, the importance of the overlap on the scanning quality was discussed [12], leading us to develop the Iso-Overlap Scan path method (ISOvScan). The originality of ISOvScan is the control of scanning quality, while minimizing measuring time, based on the control of scanning overlap. By analogy with cutting tool trajectories for which the cutter location point (C_L point) is the tool extremity [7], the sensor position is defined as C_E (Figure 1) the point which positions the digitizing line with: $\mathbf{C_O C_E} = d^* \mathbf{V_C}$. Therefore, in the part frame, the sensor trajectory is a set of configurations $(C_E; \mathbf{V_L}; \mathbf{V_C})$. To generate this trajectory, ISOvScan relies on the stretching of the 3D mesh surface which represents the part to be measured on a 2D parametric surface using the Least-Square Conformal Map (LSCM) method [14]. The n triangular facets T_j of the 3D surface are transformed into n facets t_j in the 2D space. Then, equidistant paths, each one defined by a set of driven points, are generated in the 2D space, thus transformed in the 3D space by the inverse LSCM. For each driven point, the scanner orientations are finally calculated to satisfy quality constraints. The different steps of the method are briefly detailed in the next sections.

2.1 Generation of the scanning driven points

Driven points are defined in 2D as the intersection between sucessive parallel planes and the parametric surface. To control the overlap, parallel planes are equidistant

of a value I_{2D}, corresponding to the distance between two successive paths in the 2D space (Figure 3). As the objective is to control the overlap defined by the distance I_{3D} between two successive paths in the 3D space, a relationship between I_{2D} and I_{3D} is established considering that the ratio of both values is equal to the proportionality coefficient of similar triangles T_j and t_j (Figure 3) where A_{T_j} and a_{t_j}, are the area of the facet, respectively T_j and t_j.

2.2 Generation of the scanner orientations

Scanner orientations are determined in two steps: the vector director of the digitizing line $\mathbf{V_L}$ is determined first, and then the light-beam axis $\mathbf{V_C}$. A constant scanning distance is first imposed for all the driven points to ensure that the measured surface at the driven point belongs to the Field Of View (FOV) of the scanner, and to also ensure an expected scanning quality, defined according to the scanner qualification [18]. The width of the laser line, L_{opt} associated to this scanning distance is constant with respect to the scanned surface. In order to maximize the scanned surface, the laser line must be perpendicular to the direction of displacement along the scanner trajectory in the 3D space. The laser-line width l_{opt} in the 2D space is defined from L_{opt} and using the proportionality coefficient: $l_{opt} = L_{opt}.\frac{I_{3D}}{I_{2D}}$. At each point c_{ei}, the laser-line is positioned perpendicularly to the path and centered at c_{ei} . The width l_opt defines the two end points p_{i1} and p_{i2} on the laser line (Figure 3). The coordinates of the corresponding points P_{i1} and P_{i2} are calculated using the LSCM inverse transformation. Thus, the director vector of the digitizing line $\mathbf{V_{Li}}$ at the driven point C_{Ei} is obtained from the coordinates of P_{i1} and P_{i2}. The vector of the light-beam axis $\mathbf{V_C}$ is determined so that the scanning direction is always perpendicular to the surface. The local normal vector to the surface $\mathbf{n_{C_{Ei}}}$ at each driven point C_{Ei} is calculated as the mean value of all the normal vectors to the facets related to the laser line at C_{Ei}. Finally, the director vector of the light-beam axis is defined at each driven point by: $\mathbf{V_{Ci}} = \mathbf{n_{C_{Ei}}}$.

2.3 Scanning trajectory

As the driven points are obtained by the intersection between the equidistant planes and the mesh, they are not regularly spaced. To ensure a smooth execution of the trajectory on the machine-tool, the set of driven points C_{Ei} and scanner orientations are approximated by cubic B-Spline curves in order to obtain a uniform distribution of the points independently from the mesh. The whole trajectory is thus obtained as a set of positions and orientations $(C_{Ei}; \mathbf{V_{Li}}; \mathbf{V_{Ci}})$. The scan path planning method with overlap control ISOvScan is implemented in Matlab©.

The method is applied on the surface represented in Figure 4, which is included in a volume of 100x100x30 mm^3. The sensor used is a Kreon KZ25 laser-plane (www.kreon3d.fr). This sensor has been previously characterized [11]. Its characteritics are: a laser-line width of 25 mm for a digitizing distance d^* of 50 mm from the top of FOV, a maximum view angle equal to 60°. In the example, the trajectory is calculated with a distance between passes of $I_{3D} = 15$ mm and wth

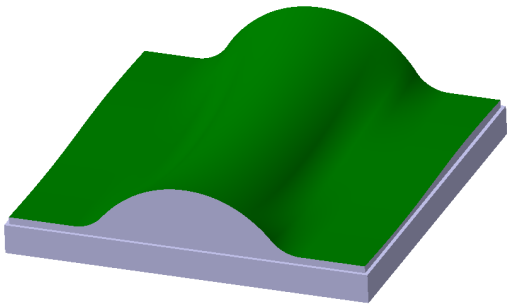

Fig. 4 Representation of the studied surface

the optimal laser linewidth of $L_{opt} = 18\ mm$. The selected overlap rate for this trajectory is 15%. The obtained trajectoiry is represented in Figure 5(a).

This scan path is first assessed by a simulator developed in a previous work[11], which relies on the analysis of the scanner configurations relatively to the meshed part. Green facets correspond to well digitized facets using only one configuration, whereas yellow facets belong to overlap zones (Figure 5(b)). The scanning simulation shows an expected digitizing result for which most facets of the surface are digitized with a good digitizing quality (in green) and the dimension of the overlap zones between the successive passes are nearly constant (in yellow).

3 Generation of the scanning trajectory for a 5-axis machine tool

The scanning trajectory obtained using the ISOvScan method is calculated in the part frame. To execute this trajectory on the 5-axis machine-tool (RRTTT architecture), the coordinates $(X, Y, Z, I, J, K, I^*, J^*, K^*)$ of each scanner configuration $(C_{Ei}; \mathbf{V_{Li}}; \mathbf{V_{Ci}})$ must be transformed into the articular configuration $(X_m, Y_m, Z_m,\ A, C, W)$ in the machine frame. This transformation is classical for 5-axis milling and is carried out using the Inverse Kinematic Transformation (IKT). The geometrical modeling of the machine tool and of the IKT are detailed in the appendix A. In the context of a scanning trajectory, this transformation must be completed, so as to take into account the sensor orientation as well as the sensor geometry. In this section, the tranformation and its resolution are presented first. Then, we detail the method that we propose to adapt to the scanning trajectory for a 5-axis machine-tool.

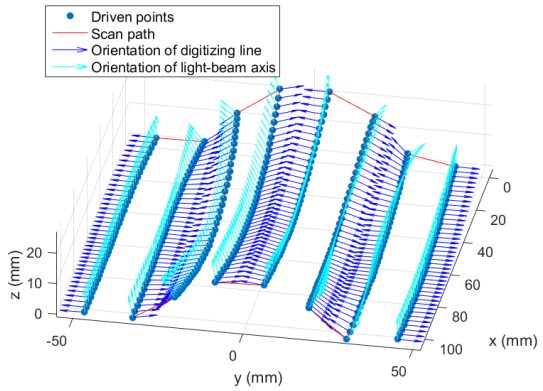

(a) Scan path generated by ISOvScan

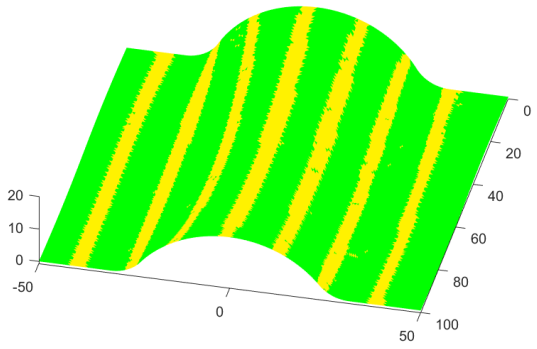

(b) Scanning simulation

Fig. 5 Scan path generated by the ISOvScan method and scanning simulation

3.1 Kinematic model of a 5-axis machine-tool with a laser-plane sensor

The main modification in the transformation expression comes from the addition of a supplementary transformation associated to the sensor frame:

$$P_{cbr} = \begin{bmatrix} R_{cbr} & T_{cbr} \\ 0 & 1 \end{bmatrix} = \begin{bmatrix} cos(W) & sin(W) & 0 & x_{O_cO_{br}} \\ -sin(W) & cos(W) & 0 & y_{O_cO_{br}} \\ 0 & 0 & 1 & z_{O_cO_{br}} \\ 0 & 0 & 0 & 1 \end{bmatrix} \quad (1)$$

where P_{cbr} is the transformation matrix between the sensor frame and the spindle frame and W is the spindle indexation around the z-axis in the sensor frame. To simplify the representation, the initial indexation is chosen at $W_0 =$

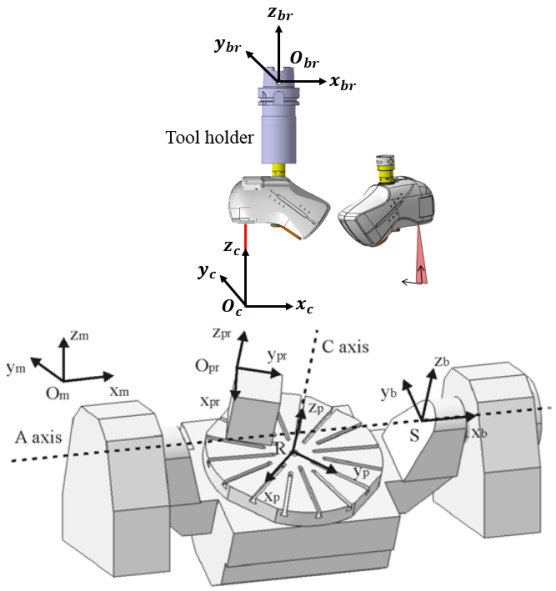

Fig. 6 Definition of machine geometry and different frames from [6]

0.Then, the tranformation from the part frame to the sensor frame is expressed from N (defined in appendix A),thanks to the transformation matrix M such as:

$$M = N.P_{cbr}^{-1} \qquad and \qquad M^{-1} = P_{cbr}.N^{-1} \tag{2}$$

The Forward Kinematics Transformation (FKT) consists in expressing the sensor configuration $(X, Y, Z,\ I, J, K,\ I^*, J^*, K^*)$ into position values of the machine axes $(X_m, Y_m, Z_m,\ A, C, W)$. The director vector of the light-beam axis $\mathbf{V}_C(I^*, J^*, K^*)$ is expressed by Equation 3:

$$\begin{bmatrix} I^* \\ J^* \\ K^* \\ 0 \end{bmatrix}_{(O_{pr}, x_{pr}, y_{pr}, z_{pr})} = M. \begin{bmatrix} 0 \\ 0 \\ 1 \\ 0 \end{bmatrix}_{(O_c, x_c, y_c, z_c)} \tag{3}$$

The director vector of the laser line $\mathbf{V}_L$ in the part frame is given by Equation 4:

$$\begin{bmatrix} I \\ J \\ K \\ 0 \end{bmatrix}_{(O_{pr}, x_{pr}, y_{pr}, z_{pr})} = M. \begin{bmatrix} 1 \\ 0 \\ 0 \\ 0 \end{bmatrix}_{(O_c, x_c, y_c, z_c)} \tag{4}$$

3.2 Resolution of Inverse Kinematics Transformation

In order to simplify the expression, we assume that the axes of the part frame (or programming frame) are aligned with the axes of the rotary table in the initial

configuration. P_{pr} can thus be expressed as:

$$P_{ppr} = \begin{bmatrix} 1 & 0 & 0 & x_{RO_{br}} \\ 0 & 1 & 0 & y_{RO_{br}} \\ 0 & 0 & 1 & z_{RO_{br}} \\ 0 & 0 & 0 & 1 \end{bmatrix} \tag{5}$$

We thus obtain the followig relations from Equations 3 and 4 from equations 3 and 4:

$$\begin{cases} I^* = sin(C).sin(A) \\ J^* = -cos(C).sin(A) \\ K^* = cos(A) \end{cases} \tag{6}$$

$$\begin{cases} I = cos(C).cos(W) - cos(A).sin(C).sin(W) \\ J = sin(C).cos(W) + cos(A).cos(C).sin(W) \\ K = sin(A).sin(W) \end{cases} \tag{7}$$

Solutions of the system 6 are summarized in Table 1 according to the values of (I^*, J^*, K^*).

For the machine we used (Mikron UCP 710), the rotation of the axis A is limited to the angular range $[-30°, +120°]$. Therefore, some solutions are not physically feasible, possible solutions according to the values of K^* are summurized in Table 2. Then, possible solutions to the equation 7 are: $W_1 = asin(K/sin(A))$ ou $W_2 = \pi - asin(K/sin(A))$.

3.3 Adaptation of the scanning trajectory to 5-axis machine-tools

The spindle indexation W plays a major role in the orientation of the scanning line with respect to the direction of the sensor dispacement. Nevertheless, as mentioned previously, the spindle indexation cannot be continuously controlled between two successive sensor configurations. The sensor trajectory must be transformed into $(X_m, Y_m, Z_m, A, C, W_{cst})$ where W_{cst} represents a constant value of the spindle indexation for all sensor configurations.

When fixing a constant value of the spindle indexation W_{cst}, according to the equations 6 and 7, it is not possible to transform the trajectory in the part frame into the trajectory in the machine frame which respects the sensor orientations $(\mathbf{V}_L, \mathbf{V}_C)$ obtained with the ISOvScan method. We recall that the sensor orientation is determined by the couple of vectors $(\mathbf{V}_L, \mathbf{V}_C)$, where the director vector of laser line $\mathbf{V}_L$ orientates the laser line relatively to the surface to be measured (Figure 1). In the initial trajectory, the vector $\mathbf{V}_L$ is perpendicular to the displacement direction along the sensor trajectory. The modification of vector $\mathbf{V}_L$ influences the control of the overlap between two consecutive scanning passes of the trajectory. The director vector of the light-beam axis $\mathbf{V}_C$ is determined so that the scanning direction is always perpendicular to the surface. By keeping the sensor normal to the surface, the scanning angle always belongs to the admissible scanning angle range for a given scanning quality. Setting $W = W_{cst}$ leads to either a possible loss of quality or an uncontrolled overlap. Before proposing an adaptation of the trajectory, it is necessary to choose a relevant value of W_{cst}.

3.3.1 Choice of the fixed value W_{cst}

The value of W_{cst} is defined as the angle between the digitizing laser line of the sensor and the x-axis in the machine frame. We suppose that W_{cst} belongs to the range of $(0°; 180°)$. From Equation 7, we remark that, if K is known, there are many possible values of W satisfying equation $sin(A) = K/sin(W)$ to find the angle A.

W_{cst} is chosen so that the rotary angle of the tilt around the A-axis is minimal. This criterion aims to reduce the risk of collision between the sensor and the rotary table when measurements are performed. The angular variation $\Delta A = A_{max} - A_{min}$ is minimal when $W_{cst} = 90°$ as $sin(W_{cst})$=1 (A_{max}, and A_{min}, are respectively the maximal and the minimal rotary angle of the tilt). Indeed, the angular variation $\Delta A = A_{max} - A_{min}$ shown in Figure 7 confirms this choice for W_{cst}. The minimal value of $\Delta A = 92°$ corresponds to $W_{cst} = 90°$.

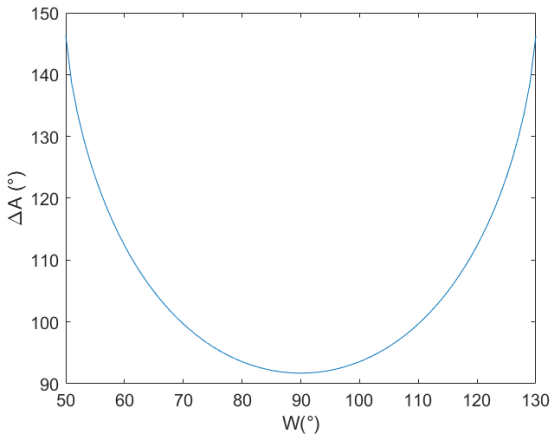

Fig. 7 Variation of A angle in function of W

The adaptation of the ISOvScan trajectory is carried out in two different ways and considering $W_{cst} = 90°$. In the first case, the adapted scanning trajectory is calculated by giving priority to measurement time, with a control of overlap, while in the second approach, prority is given to quality, with control of the sensor orientation. These two ways of trajectory adaptation are detailed in the next sections, and illustrated using the surface presented at the end of Section 2.

3.3.2 Adaption with priority of the overlap control

Priority is given to the control of overlap by maintaining the orientation of the laser line identical to the one that is calculated using the ISOvScan method. Then, the director vector of laser line $\mathbf{V}_L$ is preserved, and only the vector $\mathbf{V}_C$ is transformed into the adapted vector $\mathbf{V}_C{}'$. To do this, angles A_{ov} and C_{ov} are obtained thanks to Equation 7 using the original vector $\mathbf{V}_L$, and the chosen constant value W_{cst}.

Solutions of the system are thus obtained considering the values (I^*, J^*, K^*, W_{cst}), and the adapted vector $\mathbf{V}_C{}'$ is simply calculated thanks to the equation 8 :

$$\begin{cases} I^{*\prime} = sin(C_{ov}).sin(A_{ov}) \\ J^{*\prime} = -cos(C_{ov}).sin(A_{ov}) \\ K^{*\prime} = cos(A_{ov}) \end{cases} \tag{8}$$

The solution of system 7 are summarized in Table B according to the values of (I^*, J^*, K^*, W_{cst}) . As the rotation of the axis A is limited to the angular range $[-30°, +120°]$, some solutions are not physically feasible, and possible solutions according to the values of K are displayed in Table 4). The adapted scanning trajectory respecting the control of the overlap defined by $(C_E; \mathbf{V}_L; \mathbf{V}_C{}')$ is thus calculated. The results obtained are shown in Figure 8(a).

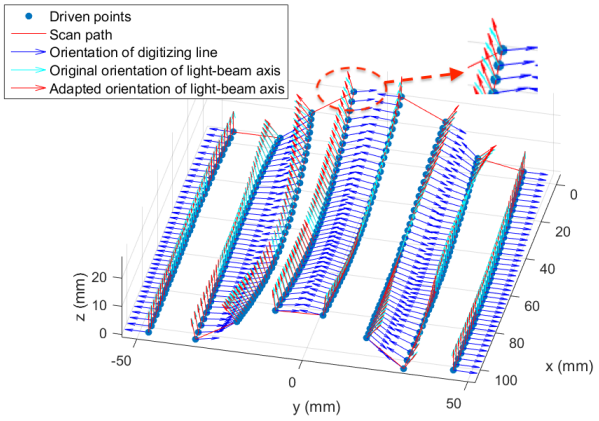

(a) Scan path with priority to the control of overlap

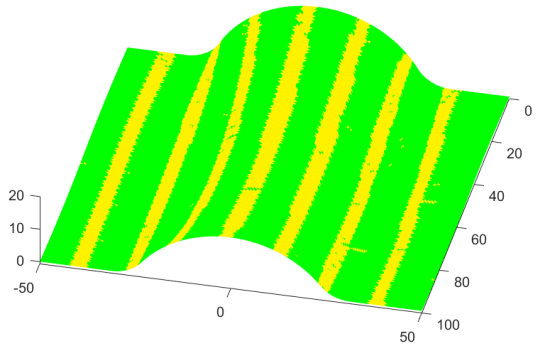

(b) Scanning simulation

Fig. 8 Scan path with priority to the overlap control and scanning simulation

Simulation results shown in Figures 5(b)and 8 highlight the good similarity between the initial trajectory calculated with ISOvScan and the adapted trajectory with priority given to the control of the overlap in terms of scanning quality and overlap areas. We note that the sizes of the overlap areas (in yellow) between the successive passes are similar to those provided for the method ISOvScan.

It seems that we can obtaine an optimal trajectory with respect to sensor orientation relative to the surface according to vector $\mathbf{V_L}$. This is due to the available large angular variation on this type of sensor for scanning quality. The angular variation between $\mathbf{V}_C{}'$ et $\mathbf{V}_C$ is displayed in Figure 9. We can see that this variation remains lower than an absolute value of 22°. This ensures that the scanning angle is always smaller than the scanning angle limit (60° for such a sensor) related to visibility and quality criteria.

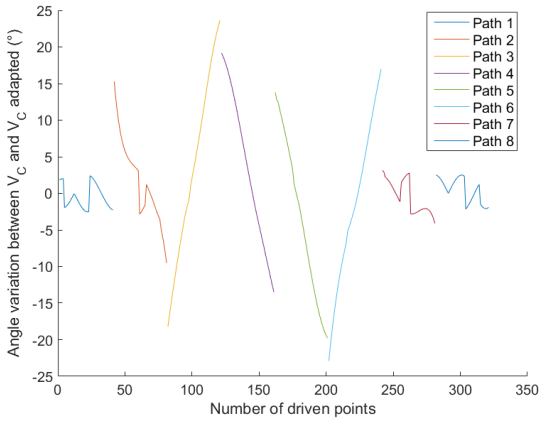

Fig. 9 Angular variation between $\mathbf{V_C}$ and $\mathbf{V'_C}$

3.3.3 Adapted scan path with priority to the scanning quality

The adapted scanning trajectory with priority to the scanning quality is carried out by conserving the orientation of the director vector of light-beam axis $\mathbf{V}_C$, and by calculating the adapted director vector $\mathbf{V}_L{}'$ representing the scanning line. The angles A and C are calculated from the original vector $\mathbf{V}_C$ using Equation 6. The adapted vector $\mathbf{V}_L{}'$ is then calculated with Equation 9 and the found values (A_q, C_q). The adapted trajectory is presented in Figure 10(a).

$$\begin{cases} I' = cos(C_q).cos(W_{cst}) - cos(A_q).sin(C_q).sin(W_{cst}) \\ J' = sin(C_q).cos(W_{cst}) + cos(A_q).cos(C_q).sin(W_{cst}) \\ K' = sin(A_q).sin(W_{cst}) \end{cases} \tag{9}$$

Although the director vector of the light-beam axis $\mathbf{V}_C$ remains unchanged from the initial scanning trajectory, it is easy to see that there are large variations between $\mathbf{V}_L{}'$ and $\mathbf{V}_L$ in Figure 10(a). The evolution of angular variations between

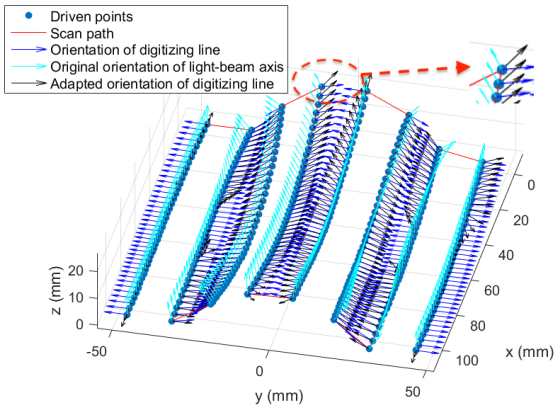

(a) Scan path with priority to the control of scanning quality

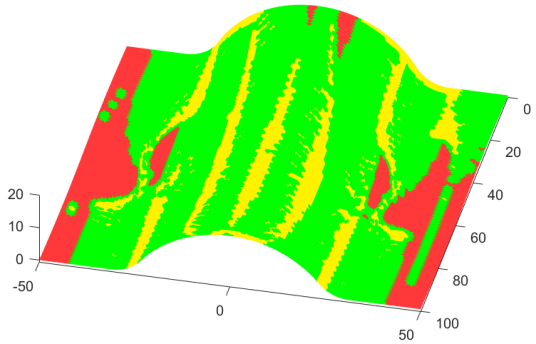

(b) Scanning simulation

Fig. 10 Scan path with priority to the scanning quality control and scanning simulation

$\mathbf{V}_L{}'$ et $\mathbf{V}_L$ presented in Figure 11 shows that the maximum variation corresponds to an absolute value of 89°. These large variations strongly affect the overlap during the scanning, and lead to many non-digitized areas on the surface (represented in red) as shown in Figure 10(b). In these areas, the orientation of the laser line is almost perpendicular to the displacement, which induces non-digitized areas.

4 Application on an industrial mahine-tool

In order to show the relevance of our method, we propose to develop a scanning application on an industrial machine-tool.

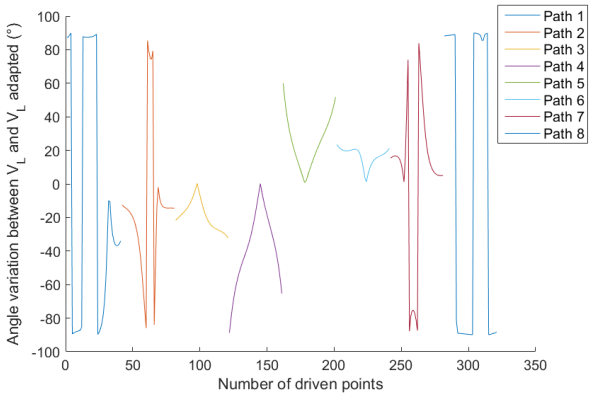

Fig. 11 Angular variations between $\mathbf{V_L}$ and $\mathbf{V'_L}$

For this application, tests are conducted in the machine-tool environment[1] using the part defined in Figure 4. This part is included in a 100x100x30 mm^3 bounding box. The workpiece is machined in two operations. A roughing operation with a toric tool, then a finishing operation with a hemispherical tool. The machining paths of the finishing operations are calculated with a machining tolerance of 5 μm and a scallop-height of 5 μm.

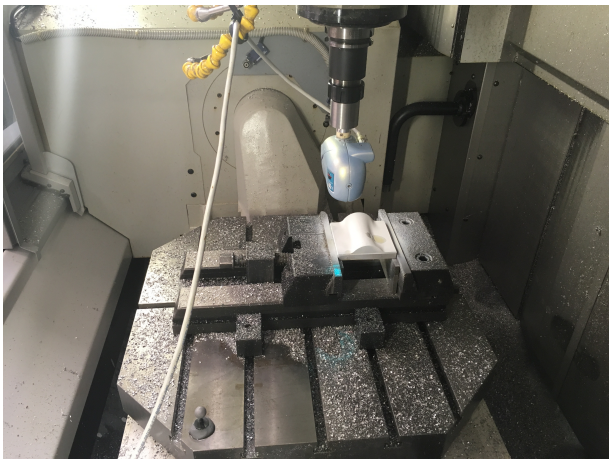

Fig. 12 Laser-plane sensor measuring in the machine-tool

The *on machine* system used consists of the Zephyr II laser-plane sensor[2] mounted in the spindle of the machine-tool with a dedicated set-up and a standard HSK 63A tool holder attachment (Figure 12). The geometrical characteristics of

[1] Mikron UCP710
[2] www.kreon3d.com

the sensor, i.e the position of the point O_c in the spindle frame are identified by the measurement of previously identified elements(elements of the table) in the working space of the machine. This yields:

$$\begin{bmatrix} x_{O_cO_{br}} \\ y_{O_cO_{br}} \\ z_{O_cO_{br}} \end{bmatrix} = \begin{bmatrix} -4.283 \\ 52.500 \\ 360.608 \end{bmatrix} \tag{10}$$

In this measurement context, the sensor qualification is determined according to the evolution of the digitizing noise, which is assessed by scanning a reference plane for different distances and view angles ([11]). According to this protocol carried out using the laser-plane sensor, the noise is less than 0.015 mm for the admissible scanning distances [20;50] mm from the bottom of FOV and the admissible view angles [0°,60°]. This value could be used as threshold value for data analysis.

4.1 Sensor calibration

To perform the measurement, we first need to calibrate the sensor. The calibration of the laser-plane sensor is carried out to determine the sensor orientation relatively to the machine frame, and to define the origin of measuring frame in which the digitized points will be expressed. The procedure of calibration involves the scanning of a measuring artefact, usually a sphere. The origin of the measuring frame is defined by the center of this reference sphere. This step is performed directly using the Polygonia software. For this purpose, it is first necessary to identify the position of the reference sphere in the frame linked to the rotary table to define the structure of the machine in the software. Once the sensor is calibrated, the scanning trajectory can be executed on the machine-tool.

4.2 Trajectory execution in 5-axes

The execution of a 5-axis trajectory on a machine-tool can be relatively complex. The most common way to facilitate programming is to use NC (Numerical controller) functions which give the trajectory directly in the part frame. These functions depend on the Numerical controller (NC) used. For a Siemens NC (840d), the TRAORI function computes the spatial transformation between the part frame and the machine frame. To make the most of use of the TRAORI function, it is necessary to define the position and the orientation of the programming frame in the working space of the machine-tool, as well as the tool length offset. Whatever the actual geometry of the tool used, it is still defined in terms of revolution geometry, based solely on length and radius. This is not the case for our sensor. It is then necessary to modify the previously calculated trajectory.

The transformation matrix N^* is introduced such as:

$$N = P_{ppr}^{-1}.P_{bp}^{-1}.P_{mb}^{-1}.P_{brm}^{-1} = N^*.P_{brm}^{-1}. \tag{11}$$

avec

$$N^* = \begin{bmatrix} R_{N^*} & T_{N^*} \\ 0 & 1 \end{bmatrix} \tag{12}$$

From the definition of M (Equation 2), we can deduce:

$$\begin{bmatrix}0\\0\\0\\1\end{bmatrix}_{(O_c,x_c,y_c,z_c)} = P_{cbr}.P_{brm}.(N^*)^{-1}.\begin{bmatrix}X\\Y\\Z\\1\end{bmatrix}_{(O_{pr},x_{pr},y_{pr},z_{pr})} \tag{13}$$

$$\begin{bmatrix}X\\Y\\Z\\1\end{bmatrix} = \begin{bmatrix}T_{pr}\\1\end{bmatrix} \tag{14}$$

After simplification, Equation 13 becomes:

$$\begin{bmatrix}0\\0\\0\end{bmatrix} = R_{cbr}.\left(\left({R_{N^*}}^t.T_{pr} - R_{N^*} * T_{N^*}\right) + T_{brm}\right) + T_{cbr} \tag{15}$$

$$T_{brm} = -{R_{N^*}}^t.T_{pr} + {R_{N^*}}^t * T_{N^*} - {R_{cbr}}^t.T_{cbr} \tag{16}$$

As R_{cbr} is a rotation around z_c, the previous equation can be written:

$$T_{brm} = -{R_{N^*}}^t.T_{pr} + {R_{N^*}}^t * T_{N^*} - \begin{bmatrix}0\\0\\z_{O_cO_{br}}\end{bmatrix} - {R_{cbr}}^t.\begin{bmatrix}x_{O_cO_{br}}\\y_{O_cO_{br}}\\0\end{bmatrix} \tag{17}$$

The TRAORI function presented in the NC Siemens 840d [25] allows spatial correction to be realized during continuous 5-axis machining. It only works for a tool geometry giving an offset according to z_{br}. In that case, because of the sensor geometry and its installation in the spindle, it is necessary to shift the coordinates of the driven points in the programming frame by a shift value $\boldsymbol{\delta}$, which depends on the sensor orientation in the machine tool frame.

$$T_{brm} = -{R_{N^*}}^t.(T_{pr} + \boldsymbol{\delta}) + {R_{N^*}}^t * T_{N^*} - \begin{bmatrix}0\\0\\z_{O_cO_{br}}\end{bmatrix} - {R_{cbr}}^t.\begin{bmatrix}x_{O_cO_{br}}\\y_{O_cO_{br}}\\0\end{bmatrix} \tag{18}$$

$$T_{brm} = -{R_{N^*}}^t.T_{pr} + {R_{N^*}}^t * T_{N^*} - \begin{bmatrix}0\\0\\z_{O_cO_{br}}\end{bmatrix} - {R_{N^*}}^t.\boldsymbol{\delta} - {R_{cbr}}^t.\begin{bmatrix}x_{O_cO_{br}}\\y_{O_cO_{br}}\\0\end{bmatrix} \tag{19}$$

This definition suggests that :

$$\boldsymbol{\delta} = -R_{N^*}.{R_{cbr}}^t.\begin{bmatrix}x_{O_cO_{br}}\\y_{O_cO_{br}}\\0\end{bmatrix} \tag{20}$$

By applying this transformation to all the points of the scan path, it is then possible to execute it on the machining center using the 5-axis machining functions. It is necessary to determine the sensor position in the machine frame in order that digitizing line position corresponds to the optimal laser linewidth L_{opt} defined in the scan path calculated using ISOvScan.

4.3 Experimental validation

The adapted scan path (with priority given to overlap control) is executed on the 5-axis machine-tool. The obtained point cloud is then registered to the CAD model of part.

The evolution of the actual scanning noise is reported in Figure 13(a), in which the scale of colors accounts for scanning noise evolution. Scanning noise is calculated for each facet of the mesh model [11]. To do this, we create a cylinder whose basis is the triangle that defines the facet. The digitized points which belong to this cylinder are represented for the actual digitized facet. The standard deviation of the digitized points distribution is then calculated for the scanning noise. We can note that digitizing noise in the overlap zones (yellow zones) is higher than that on non-overlap zones. To illustrate the proposed method, the facets are characterized in terms of scanning quality. We consider that the noise value of 0.015 mm is a threshold for quality (Figure 13(b)) according to previously defined sensor characteristics. If the noise is greater than the threshold $\sigma_{ad} = 0.015mm$, the quality of the facet is labeled as "poor", and its color is set to orange. Conversely, if the noise is less than σ_{ad}, the quality of the facet is labeled as "good", and its color is green.

The scanning quality of the measured part measurement (Figure 13(b)), as it showsthe expected result: a good scanning quality except in overlap zones. These overlap zones are relatively constant and similar to the result obtained using simulations. This validates the approach used for the generation of scanning trajectory with control of the overlap but also of the quality.

However, the analysis of geometrical deviations of the digitized data from the nominal model (Figure 14) reveals some errors during the scanning. These errors mainly come from calibration errors of the scanning system. Indeed, the scanning trajectories are performed with various machine configurations (C = 0° and C = 180° for example). Calibration errors are found to be amplified and may cause significant differences on the acquired data (zones in red on the surface). These geometrical errors may also result from the calibration process. Furthermore, as mentioned in [12], variations of scanner orientations between the passes clearly have an influence on scanning quality.

In order to illustrate the contribution of our approach, the result of the 5-axis scanning is compared with the 3-axis scanning. In this case, the surface position is fixed to the table at the position A = 0° and C = 0°. The test part is digitized with a zig-zag scan path, and the result is shown in Figure 15. Since we can not manage both the sensor orientation and the scanning distance at each driven point with the 3-axis zigzag path, the width of the overlap zone is not the same for the whole surface. Moreover, this width is larger than that of the 5-axis scan path. This illustrates the interest of our approach for digitization on 5-axis machine tools

5 Conclusion

In the context of on-machine inspection in a 5-axis machine-tool, the use of scan path planning to obtain the geometry of the surface in an optimal time with a given scanning quality is still a challenge. In this paper, we proposed a trajectory

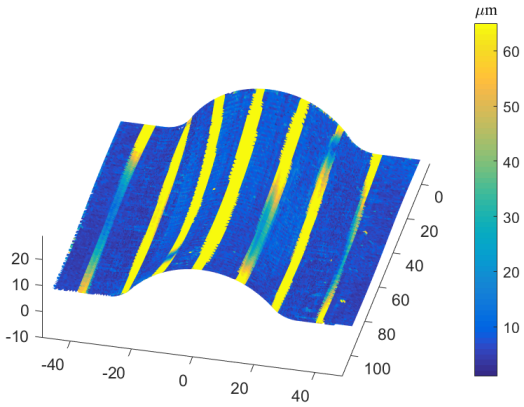

(a) Digitizing noise representation

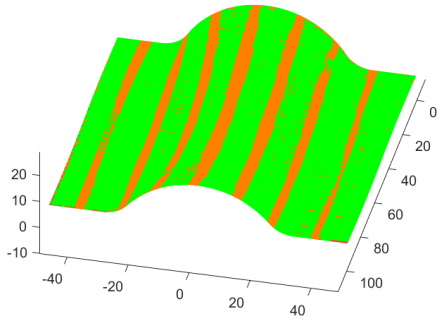

(b) Scanning quality

Fig. 13 Digitizing results analyse

planning method for a laser-plane sensor adapted to 5-axis machine-tool. This 5-axis scanning trajectory is an adaption from a previous method (ISOvScan) that was developed for laser-scanning on a robot. The originality of the ISOvscan is that it can control scanning quality and measuring time based on the control of the scanning overlap between two consecutive passes. As the kinematics of the machine-tool does not allow us to directly implement the initial scan path, it must be adapted by fixing a constant value W_{cst} for spindle indexation. Fixing a constant value W_{cst} for all the sensor configurations of the path may cause a loss of scanning quality or the control of overlap. It is therefore necessary to propose an adaptation of the trajectory by two different ways: the value is fixed considering either prority is given to quality through overlap control, or priority to time measurement through sensor orientation control. The results of the simulation and the experiment confirm the relevance of trajectory adaptation, with the adapted scan

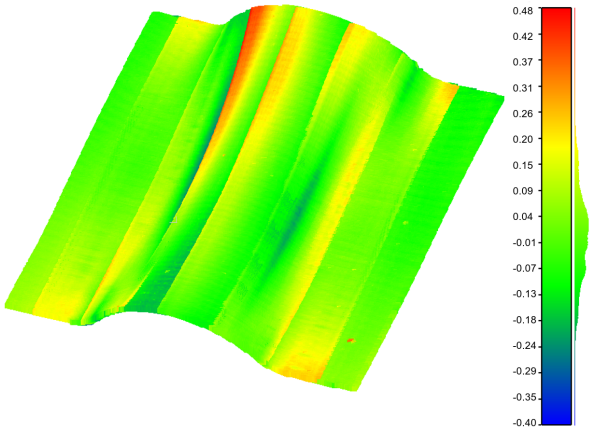

Fig. 14 Deviation representation (in mm)

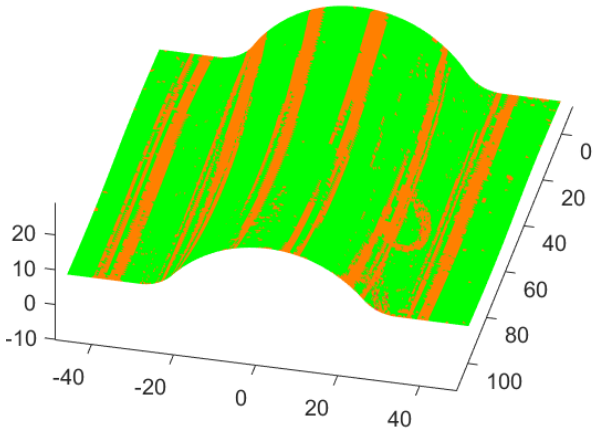

Fig. 15 Scanning quality

path with priority given to overlap control. Through this experiment, we were able to assess the benefits of the ISOvScan method and the scan path adaptation for 5-axis machine-tools. The feasability of on-machine measurement using a laser-plane was thus validated.

Future work will be dedicated on the application and deepest evaluation of adapted scan path for 5-axis machine-tool with an industrial case. Comparison with scanning result obtained with industrial robot will be also achieve.

References

1. Cho, M.W., Seo, T.I., Inspection planning strategy for the on-machine measurement process based on cad/cam/cai integration. The International Journal of Advanced Manufacturing Technology 19(8), 607617 (2002)

2. Li-jun Ding, Shu-guang Daia, Ping-an Mua, CAD-Based Path Planning for 3D Laser Scanning of Complex Surface, Procedia Computer Science, Volume 92, 2016, Pages 526-535
3. N. Huang, C. Yin, L. Liang, J. Hu, S. Wu, Error compensation for machining of large thin-walled part with sculptured surface based on on-machine measurement, The International Journal of Advanced Manufacturing Technology, Volume 96, Issue 912, pp 43454352, (2018)
4. S. Ibaraki, S. Goto, K., Tsuboi, N. Saito, N. Kojima, Kinematic modeling and error sensitivity analysis for on-machine five-axis laser scanning measurement under machine geometric errors and workpiece setup errors, The International Journal of Advanced Manufacturing Technology, Volume 96, Issue 912, pp. 40514062 (2018)
5. Imkamp, D.; Berthold, J.; Heizmann, M.; Kniel, K.; Peterek, M.; Schmitt, R.; Seidler, J.; Sommer, K.-D. Challenges and trends in manufacturing measurement technology-the Industrie 4.0 concept. J. Sens. Sens. Syst. 2016, 83, 325335.
6. Lavernhe, S., Tournier, C., and Lartigue, C. Kinematic performances in 5-axis machining. Advances in Integrated Design and Manufacturing in Mechanical Engineering II, pp. 489-503, (2007).
7. S. Lavernhe, Y. Quinsat, C. Lartigue, Model for the prediction of 3D surface topography in 5-axis milling, International Journal of Advanced Manufacturing Technology, 51, pp. 915924 (2010).
8. Mears L, Roth JT, Djurdjanovic D, Yang X, Kurfess T. Quality and Inspection of Machining Operations: CMM Integration to the Machine Tool. ASME. J. Manuf. Sci. Eng., 131(5), (2009)
9. U. Mutilba, E. Gomez-Acedo, G. Kortaberria, A.Olarra, J. A. Yague-Fabra, Traceability of On-Machine Tool Measurement: A Review, Sensor 17(7), (2017)
10. S. Nishikawa, K. Ohno, M. Mori, M. Fujishima, Non-contact Type On-machine Measurement System for Turbine Blade, Procedia CIRP, Volume 24, pp. 1-6, (2014)
11. Phan, N. D. M., Quinsat, Y., Lartigue, C. , Simulation of laser-sensor digitizing for on-machine part inspection. In Advances on Mechanics, Design Engineering and Manufacturing, pp. 301-311, (2017)
12. Phan, N.D.M, Quinsat, Y., Lavernhe, S., Lartigue, C., Scanner path planning with the control of overlap for part inspection with an industrial robot, The International Journal of Advanced Manufacturing Technology, pp. 1-15, (2018)
13. Poulhaon, F., Leygue, A., Rauch, M., Hascoet, J.Y., Chinesta. F.: Simulation-based adaptative toolpath generation in milling processes. International Journal of Machining and Machinability of Materials, 15(3-4):263284, 2014.
14. Bruno, L., Petitjean, S., Ray, N., Maillot, J.: Least squares conformal maps for automatic texture atlas generation. ACM Transactions on Graphics (TOG), 21(3):362371, (2002)
15. Besić, I., Gestel, N. V., Kruth, J.-P., Bleys, P., and Hodolić, J. (2011). Accuracy improvement of laser line scanning for feature measurements on CMM. Opt. Lasers Eng., 49(11) :12741280.
16. Quinsat, Y., Dubreuil, L., Lartigue, C.: A novel approach for in-situ detection of machining defects. The International Journal of Advanced Manufacturing Technology, 90(5-8):16251638, 2017.
17. Savio E, De Chiffre L, Schmitt R (2007) Metrology of freeform shaped parts. CIRP Ann Manuf Technol 56(2):810835
18. Mehdi-Souzani, C., Quinsat, Y., Lartigue, C., Bourdet, P.: A knowledge database of qualified digitizing systems for the selection of the best system according to the application. CIRP Journal of Manufacturing Science and Technology, 13:1523, (2016)
19. Schwenke H, Neuschaefer-Rube U, Pfeifer T, Kunzmann (2002) Optical methods for dimensional metrology in production engineering. CIRP Ann Manuf Technol 51(2):685 699
20. H. Zhao, J.-P. Kruth, N. V. Gestel, B. Boeckmans, P. Bleys, Automated dimensional inspection planning using the combination of laser scanner and tactile probe, Measurement, 45(5), pp.1057–1066 (2012).
21. ZHAO Bohan, GAO Feng, LI Yan, ZHANG Dongya,ZHANG Wanli, ZHOU Fei, Study on Generation and Optimization Methodology of On-Machine Measurement Schemes for Multi-Axis CNC Machine Tool, Proceedings of the ASME 2017 International Mechanical Engineering Congress and Exposition IMECE2017, (2017)
22. Lartigue, C., Quinsat, Y., Mehdi-Souzani, C., Zuquete-Guarato, A., Tabibian, S.: Voxel-based path planning for 3d scanning of mechanical parts. Computer-Aided Design and Applications, 11(2):220227, 2014.
23. Bernard, A., Vron, M.: Visibility theory applied to automatic control of 3d complex parts using plane laser sensors. CIRP Annals - Manufacturing Technology, 49(1):113 118, 2000.

24. Prieto, F., Redarce, H.T, Lepage, R., Boulanger, P.: Range image accuracy improvement by acquisition planning. In Proceedings of the 12th conference on vision interface, Trois Rivieres, Qubec, Canada, pages 1821, 1999.
25. Siemens, SINUMERIK 5-axis machining, Edition 05/2009 (2009)
26. Son, S., Park, H., Lee, K.H.: Automated laser scanning system for reverse engineering and inspection. International Journal of Machine Tools and Manufacture, vol. 42, no. 8, pp. 889897, 2002.
27. Mahmud, M., Joannic, D., Roy, M, Isheil, A., Fontaine, J.-F.: 3d part inspection path planning of a laser scanner with control on the uncertainty. Computer-Aided Design, vol. 43, no. 4, pp. 345355, 2011.
28. Savio E., De Chiffre L., Schmitt R., Metrology of freeform shaped parts, CIRP Annals, Vol., no. 2, pp. 810-835, 2007.

A Modeling of the 5 axis milling machine structure

The architecture of a $CAXYZ$ machine tool for which two rotations are applied to the part, and the tool orientation is fixed in the machine frame is discribed in Figure 6.

The different frames are defined from the architecture of the machine [6]:

- The spindle frame $(O_{br}, x_{br}, y_{br}, z_{br})$ is linked to the spindle (tool),
- The machine frame (O_m, x_m, y_m, z_m) is linked to the machine structure; its axes are parallel to the XYZ axes; z_m is parallel to the tool axis,
- The tilt frame (S, x_b, y_b, z_b) is linked to the tilt table; xb is parallel to x_m, S is located on the A axis,
- The table frame (R, x_p, yp, z_p) is linked to the rotary table; z_p is parallel to z_b, R is defined as the intersection between the C axis and the upper face of the table;
- The programming frame $(O_{pr}, x_{pr}, y_{pr}, z_{pr})$ is linked to the part, which represents the frame used for scan path planning.

To transform between different frames, we define the matrix that converts a vector expressed in the one frame into another frame:

$$P_{brm} = \begin{bmatrix} I_3 & T_{brm} \\ 0 & 1 \end{bmatrix} = \begin{bmatrix} 1 & 0 & 0 & x_{O_{br}O_m} \\ 0 & 1 & 0 & y_{O_{br}O_m} \\ 0 & 0 & 1 & z_{O_{br}O_m} \\ 0 & 0 & 0 & 1 \end{bmatrix} \tag{21}$$

P_{brm} is the transformation matrix between the spindle frame and the machine frame and

$$P_{mb} = \begin{bmatrix} 1 & 0 & 0 & x_{O_mO_S} \\ 0 & cos(A) & sin(A) & y_{O_mO_S} \\ 0 & -sin(A) & cos(A) & z_{O_mO_S} \\ 0 & 0 & 0 & 1 \end{bmatrix} \tag{22}$$

P_{mb}, the transformation matrix between the machine frame and the tilt frame.

$$P_{bp} = \begin{bmatrix} cos(C) & sin(C) & 0 & x_{SR} \\ -sin(C) & cos(C) & 0 & y_{SR} \\ 0 & 0 & 1 & z_{SR} \\ 0 & 0 & 0 & 1 \end{bmatrix} \tag{23}$$

Where P_{bp} is the transformation matrix between the tilt frame and the rotary table frame.

$$P_{ppr} = \begin{bmatrix} a & d & g & x_{RO_{br}} \\ b & e & h & y_{RO_{br}} \\ c & f & i & z_{RO_{br}} \\ 0 & 0 & 0 & 1 \end{bmatrix} \tag{24}$$

P_{ppr} is the transformation matrix between the rotary table frame and the part frame. The kinematic transformation matrix N from the spindle to the part is then defined as following:

$$N = P_{ppr}^{-1}.P_{bp}^{-1}.P_{mb}^{-1}.P_{brm}^{-1}. \tag{25}$$

The matrix M^{-1} is define as the transformation from the part frame to the spindle frame:

$$N^{-1} = P_{brm}.P_{mb}.P_{bp}.P_{ppr} \tag{26}$$

B Solutions of the IKT for Mikron UCP 710

Table 1 Angle solution areas A,C

	$I^* < 0$	$I^* = 0$	$I^* > 0$
$J^* < 0$	$A_1 = acos(K^*) \quad C_1 = -atan(I^*/J^*)$ $A_2 = -acos(K^*) \quad C_2 = -atan(I^*/J^*) + \pi$		
$J^* = 0$	$A_1 = acos(K^*) \quad C_1 = -\pi/2$ $A_2 = -acos(K^*) \quad C_2 = \pi/2$	$A = 0$ C not defined	$A_1 = acos(K^*) \quad C_1 = \pi/2$ $A_2 = -acos(K^*) \quad C_2 = -\pi/2$
$J^* > 0$	$A_1 = acos(K^*) \quad C_1 = -atan(I^*/J^*) + \pi$ $A_2 = -acos(K^*) \quad C_2 = -atan(I^*/J^*)$		

Table 2 Solution as a function of K^*

Value of K^*	[-1, -0.5[	[-0.5, 0.866[	[0.866,1[	1
Number of solution	0	1	2	∞
Solutions	$\emptyset$	(A_1, C_1)	(A_1, C_1) o (A_2, C_2)	A=0° and C indifferent

C Solutions of the IKT for Mikron UCP 710

Notation : $a_{ov} = asin(K/sin(W_{cst}))$, $c_{ov} = acos(cos(W_{cst})/\sqrt{1-K^2})$

Table 3 Angle solution areas A,C

	$J < 0$	$J = 0$	$J > 0$
$I < 0$	$A_{ov_1} = a_{ov}$ $C_{ov_1} = atan(J/I) + c_{ov}$ $A_{ov_2} = \pi - a_{ov}$ $C_{ov_2} = \pi + atan(J/I) + c_{ov}$		
$I = 0$	$A_{ov_1} = a_{ov}$ $C_{ov_1} = \pi/2 + c_{ov}$ $A_{ov_2} = \pi - a_{ov}$ $C_{ov_2} = -\pi/2 + c_{ov}$	$A = 90°$ C not defined	$A_{ov_1} = a_{ov}$ $C_{ov_1} = -\pi/2 + c_{ov}$ $A_{ov_2} = \pi - a_{ov}$ $C_{ov_2} = \pi/2 + c_{ov}$
$I > 0$	$A_{ov_1} = a_{ov}$ $C_{ov_1} = atan(J/I) - c_{ov}$ $A_{ov_2} = \pi - a_{ov}$ $C_{ov_2} = \pi + atan(J/I) - c_{ov}$		

Table 4 Solution as a function of K

Value of K	[-1, -0.5[	[-0.5, 0.866[	[0.866,1[	1
Number of solution	0	1	2	∞
Solutions	$\emptyset$	(A_{ov_1}, C_{ov_1})	(A_{ov_1}, C_{ov_1}) o (A_{ov_2}, C_{ov_2})	$A = 90°$ and C indifferent